Plasmon-Enhanced Four-Wave Mixing for Superresolution Applications

Boris Simkhovich[1] and Guy Bartal[1,2,*]
[1]The Russell Berrie Nanotechnology Institute, Technion—Israel Institute of Technology, Haifa 32000, Israel
[2]Department of Electrical Engineering, Technion—Israel Institute of Technology, Haifa 32000, Israel
(Received 8 August 2013; published 7 February 2014; corrected 11 February 2014)

We introduce a nonlinear optical approach to transform spatial information stored in evanescent waves into propagating ones: we study analytically the use of partially degenerate four-wave mixing in thin metallic film to map a band of evanescent waves at a given frequency into a propagating-wave band at a different one. The relatively low efficiency of this process is compensated by setting the pump beam, mediating this transformation, to be a surface plasmon polariton, whose field enhancement increases the nonlinear interaction strength. This setting can be utilized for nonresonant plasmon-assisted superresolution applications that support transverse-electric polarization, in contrast to linear plasmonic imaging (such as superlens) that can only transfer transverse-magnetic waves.

DOI: 10.1103/PhysRevLett.112.056802 PACS numbers: 73.20.Mf, 42.65.-k

The fast developing fields of nanoscience and nanotechnology have generated a demand for the visualization of deep subwavelength targets in the visible and IR wavelength range—well beyond the Abbe diffraction limit [1]. Significant progress was reported using surface plasmon polaritons (SPPs), the modes of a metal-dielectric surface [2,3], which can achieve a very short wavelength and tight mode confinement. In his pioneering work, Pendry [4] explored the concepts of a perfect lens and a superlens, relying on surface modes in metal and negative-index material which, later on, were followed by a number of experimental realizations. While a truly perfect lens made of negative-index material has not been realized yet, a superlens at near UV was demonstrated experimentally using a 35 nm silver slab [5]. The flat optical transfer function (OTF) of the superlens, which is necessary for successful imaging, was obtained at the operation wavelengths that match the SPP resonance and only at TM polarization. Moreover, while showing resolution enhancement, the evanescent information enhanced by SPPs was recorded in the near field, making this method unusable for standard optical microscopes.

A more advanced superresolution method, termed "hyperlens," was proposed [6,7] and realized soon thereafter [8,9]. Exploiting a radially bent structured metamaterial, it was able to squeeze the evanescent wave vectors into the propagating window, thereby magnifying the object beyond the diffraction limit. While providing far-field imaging, detectable by conventional microscopy, the hyperlens is still restricted to the SPP resonance wavelength and limited to TM polarization.

A somewhat different approach [10], based on a structurally modified superlens, relies on folding an evanescent band into the propagating region, thereby enabling one-dimensional objects nearly 2 times below the diffraction limit to be successfully resolved.

Electromagnetic waves on metallic surface were also shown to both contribute to and benefit from nonlinear optical effects. For example, second harmonic generation from a silver mirror was first demonstrated in 1965 [11], whereas the role of plasmons was explored later in 1974 [12]. Third harmonic generation from metal interfaces, on the other hand, albeit being first detected in 1969 [13], has been studied with plasmonic field only recently. Using partially degenerate four-wave mixing (PDFWM) in gold, intriguing phenomena and applications such as nonlinear excitation of surface plasmons [14], nonlinear negative refraction [15], and nonlinear dark-field microscope [16] were demonstrated experimentally.

The basic idea behind those observations is the relaxation of the phase-matching condition (a key element in most nonlinear wave mixing) along the direction normal to the interface, enabled by the small penetration depth of the electromagnetic field into the metals. This provides an additional degree of freedom for the wave vectors participating in this interaction.

In this Letter, we exploit this partial phase matching along a metal-dielectric interface to introduce a new approach for delivering spatial information stored in evanescent waves: we map a large band of evanescent waves into a propagating waves band by PDFWM. The relatively low efficiency of this process is compensated by setting the pump beam to be SPP, whose field enhancement increases the nonlinear interaction strength. This setting can map an evanescent wave to a propagating one at both polarizations (with different OTF), giving rise to plasmonic-assisted superresolution applications at TE polarization. This differs significantly from linear plasmonic imaging (such as the superlens) transferring only TM waves.

Partially degenerate FWM [17] is a third-order nonlinear process involving a pump field contributing two photons

for each interaction and a signal field stimulating the codirectional emission of the photon at ω_2. As a result, an additional photon at a frequency ω_{FWM} emerges. In this work, we set the pump field to be a surface plasmon; hence, it will be referred to as $\vec{E}_{pl}(\omega_1)$, where the signal field is $\vec{E}_{\mathrm{sig}}(\omega_2)$ and the newly generated field is $\vec{E}(\omega_{\mathrm{FWM}})$. Assuming that all the mixing waves are plane waves (including nonhomogeneous evanescent waves), the FWM field is generated by the nonlinear polarization, which acquires the form

$$P_i^{\mathrm{NL}}(\omega_{\mathrm{FWM}},\vec{k}_{\mathrm{NL}}) = \chi^{(3)}_{ijkl}(\omega_{\mathrm{FWM}};\omega_1,\omega_1,-\omega_2)E_{pl,j}(\omega_1,\vec{k}_{pl}) \times E_{pl,k}(\omega_1,\vec{k}_{pl})E^*_{\mathrm{sig},l}(\omega_2,\vec{k}_{\mathrm{sig}}) + c.c., \quad (1)$$

where the complex conjugate field presentation indicates stimulated photon generation and the indices (i, j, k, l) correspond to the x-y-z Cartesian axes. The conservation of energy and momentum determines ω_{FWM} and $\vec{k}_{\mathrm{FWM}}$:

$$\omega_{\mathrm{FWM}} = 2\omega_1 - \omega_2, \quad (2)$$

$$\vec{k}_{\mathrm{FWM}} = 2\vec{k}_1 - \vec{k}_2. \quad (3)$$

Assuming nondepleted signal and pump fields, the nonlinear wave equation for the newly generated frequency ω_{FWM} decouples from those of the pump and signal fields, with the nonlinear polarization acting as a source term (Ref. [17]):

$$\left[\nabla\times(\nabla\times) - \frac{\omega^2_{\mathrm{FWM}}\varepsilon(\omega_{\mathrm{FWM}})}{c^2}\right]\vec{E}(\omega_{\mathrm{FWM}}) = \frac{\omega^2_{\mathrm{FWM}}}{\varepsilon_0 c^2}\vec{P}^{\mathrm{NL}}(\omega_{\mathrm{FWM}}). \quad (4)$$

The above nonhomogeneous equation is linear and therefore phasor representation of the FWM fields can be used; hence, we omit the complex conjugate terms of the fields from our calculations.

Generally, an efficient nonlinear conversion in a bulk of nonlinear medium requires conservation of momentum [Eq. (3)], which typically conflicts with the medium's linear dispersion relations. Hence, it is difficult to obtain full phase-matching conditions, especially in dispersive media. However, for a thin film of a nonlinear medium, with thickness L much smaller than the wavelength, the accumulated mismatch in the normal to the film direction is negligible ($\Delta kL \ll \pi$, Δk being the momentum mismatch normal to the interface). Therefore, the requirement of matching wave vector components normal to the film is relaxed. This scenario is termed the "partially phase-matched process" and, interestingly, enables any wave vector combination on the left-hand side of Eq. (3) to result in a nonlinear polarization with a corresponding wave vector $\vec{k}_{\mathrm{FWM}}$, which is determined solely by Eq. (3). At the same time, the new FWM field that is coupled out of the nonlinear source will propagate with a wave vector having a tangential component equal to $\vec{k}_{\mathrm{FWM}}$ and a normal component determined by the medium's linear dispersion relation [18]. Such a field constitutes a homogeneous solution of Eq. (4) and could be propagating or evanescent. While the partial phase matching is generally valid for both dimensions of the interface, in this Letter we limit ourselves to surface plasmon and signal wave vectors, $\vec{k}_1$ and $\vec{k}_2$, lying in the same plane of incidence.

Such a partially phase matched PDFWM process is best represented in ω-k space, where the conserved $(\omega, k_\parallel)$ quantities ($\parallel$ means parallel to the interface) form a line segment in ω-k space: the pump field point $(\omega_1, k_{1,\parallel})$ lies in the middle of the line segment defined by its end points $(\omega_2, k_{2,\parallel})$ and $(\omega_{\mathrm{FWM}}, k_{\mathrm{FWM},\parallel})$. Figure 1(a) depicts a schematic representation of some recent observations utilizing partially phase matched PDFWM [15,19,20]. Partial phase matching was also demonstrated in multilayer graphene [21–23].

Interestingly, the partial phase-matching condition can be exploited to map an evanescent wave vector at frequency ω_2 to a propagating one at the newly generated frequency ω_{FWM}. Furthermore, as this process is not limited to a single wave vector, it allows to duplicate a band from the evanescent region in k space, $k_{2,x} > k_{2,0}$ at ω_2 into the propagating band $-k_{\mathrm{FWM},0} < k_{\mathrm{FWM},x} < k_{\mathrm{FWM},0}$ at ω_{FWM} with one-to-one mapping (where $k_{2,0} = \omega_2/c$, $k_{\mathrm{FWM},0} = \omega_{\mathrm{FWM}}/c$, and c is the speed of light in air). Namely, the pump SPP field, launched at ω_1, acts as a nonlinear transformer that converts evanescent waves band at a given frequency to propagating waves at a different frequency. Figure 1(b) provides a schematic representation of this concept.

This introduces a new way to resolve subdiffraction limited objects with some advantages over existing

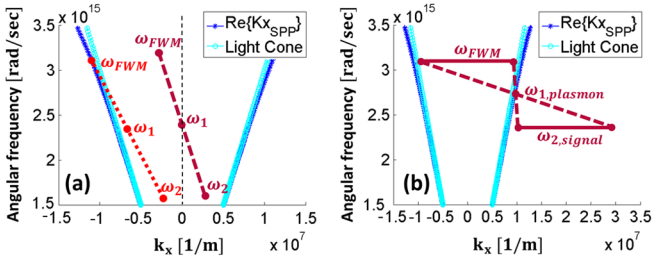

FIG. 1 (color online). ω-k diagrams of partially degenerate FWM.(a) Diagrams of experimentally observed partially phase matched PDFWM conversions. The dotted line represents conversion of propagating waves at frequencies ω_1 and ω_2 into SPP at ω_{FWM} frequency [19,20]. The dashed line represents nonlinear negative refraction, where a wave vector at frequency ω_2 is converted to a wave vector at frequency ω_{FWM} with opposite sign [15]. (b) ω-k representation of the proposed scheme utilizing PDFWM conversion to fold the evanescent region in k space $k_{2,x} > k_{2,0}$ at ω_2 into the propagating band $-k_{\mathrm{FWM},0} < k_{\mathrm{FWM},x} < k_{\mathrm{FWM},0}$ at ω_{FWM} (solid lines) with one-to-one mapping (dashed lines). The dash-dotted lines and crosses represent the light line and SPP dispersion, respectively.

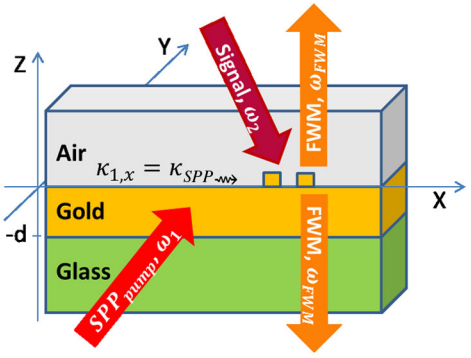

FIG. 2 (color online). Exemplification of the proposed idea: a target that consists of subwavelength features (e.g., two nanobars) is overlayed on a gold layer deposited on glass. A pump beam, illuminated through the glass, is coupled to a SPP propagating along the gold-air interface, while the signal beam illuminates the target, resulting in a multitude of evanescent waves (the Fourier decomposition of subwavelength objects) near the surface. The generated FWM wave is reflected into both air and glass media.

plasmonic superresolution techniques: broadband operation (also for TE polarization) and noise reduction due to the frequency conversion.

The proposed setup is illustrated in Fig. 2 and consists of a metallic layer deposited on a glass prism. The strong pump field (ω_1), launched from the side of the prism, is coupled to SPP by Kretschmann-like configuration, while the object lies on top of the gold interface and is illuminated from the air side by the signal laser (ω_2). The evanescent field generated by the subwavelength features of the target is converted by the nonlinear interaction to the propagating waves at the FWM frequency.

In what follows, we assume that the plasmonic pump field propagates along the $\hat{x}$ direction and the target is invariant in the $\hat{y}$ direction. This decouples the TE and TM polarizations and significantly simplifies the calculations. We use gold as the nonlinear medium, whose nonlinear third-order susceptibility contains only four nonvanishing terms due to its symmetry (χ_{kkkk}, χ_{klkl}, χ_{kkll}, χ_{kllk}), where only three of them are independent, $\chi_{kkkk} = \chi_{kkll} + \chi_{klkl} + \chi_{kllk}$. Furthermore, due to the squared plasmonic contribution, the terms χ_{klkl} and χ_{kkll} are identical. Consequently, the tensor expression, Eq. (1), for the nonlinear polarization can be simplified using the following parameters:

$$\begin{aligned} p_1 &= 3\epsilon_0(\chi_{kkkk}E_{x,pl}^2 + \chi_{kllk}E_{z,pl}^2), \\ p_2 &= 6\epsilon_0\chi_{kkll}E_{x,pl}E_{z,pl}, \\ p_3 &= 3\epsilon_0(\chi_{kllk}E_{x,pl}^2 + \chi_{kkkk}E_{z,pl}^2), \\ p_4 &= 3\epsilon_0\chi_{kllk}(E_{x,pl}^2 + E_{z,pl}^2). \end{aligned} \tag{5}$$

The nonlinear response for an arbitrary incoming signal field $\vec{E}_{\text{sig}} = (E_{x,\text{sig}}, E_{y,\text{sig}}, E_{z,\text{sig}})$ can, hence, be written in a convenient matrix representation:

$$\vec{P}^{NL}_{w_{\text{FWM}}} = \begin{bmatrix} p_1 & 0 & p_2 \\ 0 & p_4 & 0 \\ p_2 & 0 & p_3 \end{bmatrix} \begin{pmatrix} E^*_{x,\text{sig}} \\ E^*_{y,\text{sig}} \\ E^*_{z,\text{sig}} \end{pmatrix}. \tag{6}$$

The solution of Eq. (4) is a sum of homogeneous and particular solutions (the solution below closely follows the second harmonic generation solution of Ref. [18]):

$$\vec{E}(\omega_{\text{FWM}}) = \vec{E}^H(\omega_{\text{FWM}}) + \vec{E}^P(\omega_{\text{FWM}}). \tag{7}$$

The homogeneous solution $\vec{E}^H(\omega_{\text{FWM}})$ corresponds to the solution of Eq. (4) with the polarization term set to zero and constitutes the plane waves base $\vec{E}^H(\omega_{\text{FWM}}) = \vec{E}^H_0 e^{i(\vec{k}_H\cdot\vec{r}-\omega_{\text{FWM}}t)}$ with the wave vector defined by the medium dispersion $\vec{k}_H^2 = \omega_{\text{FWM}}^2\varepsilon(\omega_{\text{FWM}})/c^2$. The particular solution $\vec{E}^P(\omega)$ (oscillating as $e^{i(k_{\text{FWM}}\cdot\vec{r}-\omega_{\text{FWM}}t)}$) is found by decomposing Eq. (4) into the components parallel and normal to $\vec{k}_{\text{FWM}}$,

$$\begin{aligned} \left[\nabla^2 + \frac{\omega_{\text{FWM}}^2\varepsilon(\omega_{\text{FWM}})}{c^2}\right]\vec{E}^P_\perp &= -\frac{\omega_{\text{FWM}}^2}{\varepsilon_0 c^2}\vec{P}^{\text{NL}}_\perp, \\ \frac{\omega_{\text{FWM}}^2\varepsilon(\omega_{\text{FWM}})}{c^2}\vec{E}^P_\parallel &= -\frac{\omega_{\text{FWM}}^2}{\varepsilon_0 c^2}\vec{P}^{\text{NL}}_\parallel. \end{aligned} \tag{8}$$

Therefore, the particular solution of the above equations is

$$\begin{aligned} \vec{E}^P_\perp &= \frac{\omega_{\text{FWM}}^2}{\varepsilon_0 c^2(\vec{k}_{\text{FWM}}^2 - \vec{k}_H^2)}\vec{P}^{\text{NL}}_\perp, \\ \vec{E}^P_\parallel &= -\frac{1}{\varepsilon_0\varepsilon(\omega_{\text{FWM}})}\vec{P}^{\text{NL}}_\parallel. \end{aligned} \tag{9}$$

Summarizing both contributions, the particular solution in the nonlinear medium can be written in a compact form:

$$\begin{aligned} \vec{E}^P &= \vec{E}^P_\perp + \vec{E}^P_\parallel \\ &= \frac{\omega_{\text{FWM}}^2}{\varepsilon_0 c^2(\vec{k}_{\text{FWM}}^2 - \vec{k}_H^2)}\left(\vec{P}^{\text{NL}} - \frac{\vec{k}_{\text{FWM}}\cdot(\vec{k}_{\text{FWM}}\cdot\vec{P}^{\text{NL}})}{\vec{k}_H^2}\right). \end{aligned} \tag{10}$$

Solution of the slab geometry (two coupled interfaces illustrated in Fig. 2) requires an additional homogeneous solution reflecting the existence of the second interface, namely, $\vec{E}'^H(\omega_{\text{FWM}}) = \vec{E}'^H_0 e^{i(\vec{k}'_H\cdot\vec{r}-\omega_{\text{FWM}}t)}$, with $\vec{k}'_H$ equal to $\vec{k}_H$ but with opposite sign of the $k_{H,z}$ component (i.e., the wave decays exponentially from the second interface in the $-z$ direction). Furthermore, homogeneous solutions also exist in the surrounding dielectric media; hence the electric field in the entire space is represented by

$$\begin{aligned} \vec{E}_{D_1} &= \vec{E}_{0,D_1}e^{i(\vec{k}_{D_1}\cdot\vec{r}-\omega_{\text{FWM}}t)}, \quad z \geqq 0, \\ \vec{E} &= \vec{E}^H_0 e^{i(\vec{k}_H\cdot\vec{r}-\omega_{\text{FWM}}t)} + \vec{E}'^H_0 e^{i(\vec{k}'_H\cdot\vec{r}-\omega_{\text{FWM}}t)} + \vec{E}^P, \\ &\quad -d \leqq z < 0, \\ \vec{E}_{D_2} &= \vec{E}_{0,D_2}e^{i(\vec{k}_{D_2}\cdot\vec{r}-\omega_{\text{FWM}}t)}, \quad z < -d, \end{aligned} \tag{11}$$

where the subscripts D_1 and D_2 correspond to the surrounding dielectrics and d is the slab width. The above equation has four unknown amplitudes of the homogeneous solutions, which are determined by the boundary conditions. All other parameters are known for given plasmonic and signal plane waves, while the wave vector components parallel to the interface are conserved:

$$k_{\mathrm{FWM},x} = 2k_{1,x} - k_{2,x} = k_{H,x} = k_{D_1,x} = k_{D_2,x}; \qquad (12)$$

the wave vector components in the $\hat{z}$ direction are determined by the linear dispersion relations and by Eq. (3) for $\vec{k}_{\mathrm{FWM}}$.

Under the assumption that TE and TM polarizations decouple ($k_{\mathrm{FWM},y} = 0$), the separate boundary conditions can be written as

$$TE: \begin{bmatrix} 1 & -1 & -e^{-ik_{H,z}d} & 0 \\ -k_{D_1,z} & k_{H,z} & -k_{H,z}e^{-ik_{H,z}d} & 0 \\ 0 & e^{-ik_{H,z}d} & -1 & 1 \\ 0 & e^{-ik_{H,z}d} & -k_{H,z} & -k_{D_2,z} \end{bmatrix} \begin{pmatrix} E_{0,y,D_1} \\ E^H_{0,y} \\ E'^H_{0,y} \\ E_{0,y,D_2} \end{pmatrix}$$
$$= \begin{pmatrix} E^P_y \\ -k_{F,z}E^P_y \\ e^{-ik_{F,z}\cdot d}E^P_y \\ -k_{F,z}e^{-ik_{F,z}\cdot d}E^P_y \end{pmatrix}, \qquad (13)$$

$$TM: \begin{bmatrix} 1 & -1 & -e^{-ik_{H,z}d} & 0 \\ -\frac{\varepsilon_{D_1}k_{H,x}}{k_{D_1,z}} & \frac{\varepsilon_G k_{H,x}}{k_{H,z}} & -\frac{\varepsilon_G k_x}{k_{H,z}}e^{-ik_{H,z}d} & 0 \\ 0 & -e^{-ik_{H,z}d} & -1 & 1 \\ 0 & \frac{\varepsilon_G k_{H,x}}{k_{H,z}}e^{-ik_{H,z}d} & -\frac{\varepsilon_G k_{H,x}}{k_{H,z}} & -\frac{\varepsilon_{D_2}k_{H,x}}{k_{D_2,z}} \end{bmatrix}$$
$$\times \begin{pmatrix} E_{0,x,D_1} \\ E^H_{0,x} \\ E'^H_{0,x} \\ E_{0,x,D_2} \end{pmatrix} = \begin{pmatrix} E^P_x \\ \varepsilon_G E^P_z \\ e^{-ik_{F,z}\cdot d}E^P_x \\ \varepsilon_G e^{-ik_{F,z}\cdot d}E^P_z \end{pmatrix}. \qquad (14)$$

For compactness, the dielectric constant's dependence on frequency is omitted, ε_G is the gold dielectric constant and $\vec{k}_F = \vec{k}_{\mathrm{FWM}}$.

We estimate the efficiency of the process using the nonlinear constants of Au reported by Ref. [19]: $\chi^{(3)} = 0.2(\mathrm{nm}^2/V^2)$ and the ratio between independent tensor components $\chi_{klik}/\chi_{klkl} = 4$. To calculate the electric field amplitudes, we set the pump field intensity to be an order of magnitude below the damage threshold of gold [24], which can be achieved by a conventional pulsed laser. Estimations of the required laser intensity are shown in the Supplemental Material [25]. The dielectric constant of gold, used in the calculations, follows a parametrized model of experimental results [26] and the other two dielectrics are assumed to be dispersionless constants, $\epsilon_{D_1} = 1$ for air and $\epsilon_{D_2} = 2.25$ for glass. We set the signal beam to be at 709 nm wavelength, the FWM at 600 nm wavelength, and the plasmonic pump wavelength to be at 650 nm.

We first calculate the nonlinear OTF, i.e., the ratio between the amplitude at the FWM wavelength and that of the signal wavelength ($|E_{\mathrm{FWM}}|/|E_{\mathrm{sig}}|$) as a function of the tangential wave vector, for both polarizations. The calculation results are shown in Fig. 3 for both the FWM waves reflected to the air and those transmitted to the glass. Evidently, both TE waves (in air and in the glass) exhibit smooth OTF, making it potentially suitable for imaging. The TM polarization, exhibiting a resonant behavior, is less suitable for imaging and is further discussed in the Supplemental Material [25].

We next demonstrate the potential use of our proposed scheme for future superresolution applications at TE polarization. An object consisting of two infinite slits at 30 nm width and 155 nm distance between their centers is placed atop a 50 nm thick gold layer. Owing to the subwavelength nature of the object, its spatial Fourier decomposition, represented by a solid line in Fig. 4(a), spans well beyond the propagating waves region $-k_{2,0} < k_{2,x} < k_{2,0}$. The linear dependence of $\vec{P}^{\mathrm{NL}}$ in the signal field [Eq. (1)] allows the superposition principle and the use of Fourier decomposition. The blue circles in Fig. 4(a) represent the range of wave vectors which are mapped to the propagating waves region by the nonlinear interaction.

The reconstructed TE images, obtained by folding the evanescent band $k_{2,0} < k_{2,x} < 3k_{2,0}$ into the propagating band in air, $-k_{\mathrm{FWM},0} < k_{\mathrm{FWM},x} < k_{\mathrm{FWM},0}$, and in glass, $-k_{\mathrm{FWM},0}\sqrt{\epsilon_{D_2}} < k_{\mathrm{FWM},x} < k_{\mathrm{FWM},0}\sqrt{\epsilon_{D_2}}$, are shown in Fig. 4 [in air Fig. 4(c) and in the glass Fig. 4(d)], along with their cross sections [Fig. 4(b), dashed and dotted lines, respectively]. Notably, the object can be reconstructed and projected to air, where the spatial information is carried by propagating waves and could be imaged by conventional

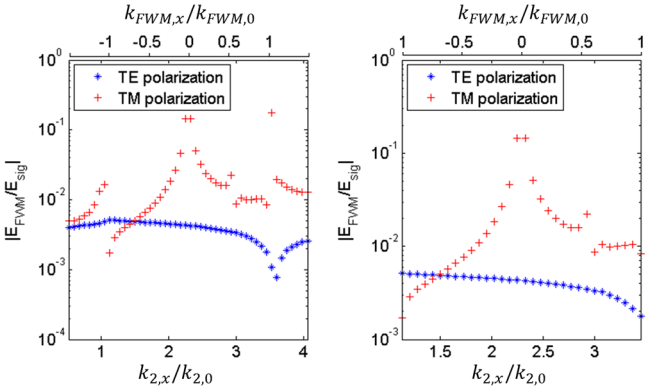

FIG. 3 (color online). OTFs in different media. Left: The OTF of the process in glass, describing how the different evanescent wave vectors will be transferred to the glass side. Red crosses, TM polarization; blue stars, TE polarization. Right: Same for the air side. Note that the range in the spatial frequencies is expanded in the glass by a ratio equal to the glass index of refraction.

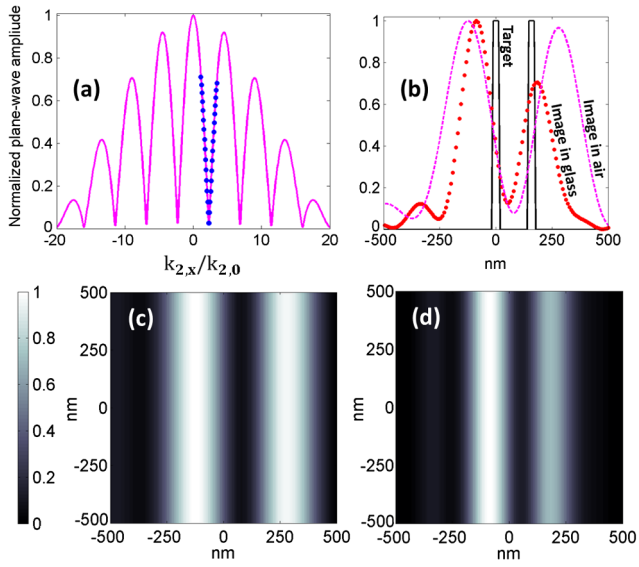

FIG. 4 (color online). Nonlinear superresolution of subwavelength target.(a) k-space representation of the Fourier decomposition of the object (solid line) along with the evanescent band that is being transformed into the propagating band by the nonlinear interaction (blue circles). (b) Cross sections of the reconstructed images at FWM wavelength (dashed and dotted lines) overlayed on the object transmission function (solid line). (c),(d) Intensity distribution of the nonlinearly transformed object (at the FWM wavelength) in air and in glass, respectively.

microscopy. Surprisingly, this process works best for TE polarization, whereas all other plasmonic superresolution schemes are limited to TM polarization. The presented results validate the feasibility of the proposed nonlinear system for future applications in far-field superresolution imaging, whereby features nearly 3 times below the diffraction limit could be resolved.

In conclusion, by mapping evanescent information into propagating waves via nonlinear wave mixing, one could resolve subdiffraction limited objects with some pronounced advantages over existing plasmonic superresolution techniques, e.g., superlens. This method is generic and could be applied in any thin nonlinear medium (provided the nonlinear interaction is strong enough), e.g., in graphene or thin graphite. The proposed concept works for TE polarization and at a broad range of wavelengths, not limited to plasmonic resonance or TM polarization. Moreover, the change in frequency assists in noise reduction in the system, where the background carried by the signal frequency can be easily filtered by a proper color filter. On the other hand, this method transforms only part of the spatial spectrum into propagating waves and, hence, does not yet provide perfect imaging. To become practical, therefore, it should be combined with other conventional imaging techniques; for example, collecting the propagating waves that transmit through the thin layer could complete the spatial information of the image.

The authors thank G. Rosenblatt for helpful discussions. This work was supported by the Israel Science Foundation (ISF), by the ICore Center "circle of light" and by the Russell Berrie Nanotechnology Institute (RBNI).

*Corresponding author.
guy@ee.technion.ac.il

[1] E. Abbe, Arch. Mikrosk. Anat. **9**, 413 (1873).
[2] S. Maier, *Plasmonics: Fundamentals and Applications* (Springer, New York, 2007).
[3] S. Kawata, Y. Inouye, and P. Verma, Nat. Photonics **3**, 388 (2009).
[4] J. Pendry, Phys. Rev. Lett. **85**, 3966 (2000).
[5] N. Fang, H. Lee, C. Sun, and X. Zhang, Science **308**, 534 (2005).
[6] A. Salandrino and N. Engheta, Phys. Rev. B **74**, 075103 (2006).
[7] Z. Jacob, L. V. Alekseyev, and E. Narimanov, Opt. Express **14**, 8247 (2006).
[8] Z. Liu, H. Lee, Y. Xiong, C. Sun, and X. Zhang, Science **315**, 1686 (2007).
[9] I. I. Smolyaninov, Y.-J. Hung, and C. C. Davis, Science **315**, 1699 (2007).
[10] Z. Liu, S. Durant, H. Lee, Y. Pikus, N. Fang, Y. Xiong, C. Sun, and X. Zhang, Nano Lett. **7**, 403 (2007).
[11] S. Jha, Phys. Rev. Lett. **15**, 412 (1965).
[12] H. Simon, D. Mitchell, and J. Watson, Phys. Rev. Lett. **33**, 1531 (1974).
[13] N. Bloembergen, W. Burns, and M. Matsuoka, Opt. Commun. **1**, 1 (1969).
[14] J. Renger, R. Quidant, N. van Hulst, S. Palomba, and L. Novotny, Phys. Rev. Lett. **103**, 266802 (2009).
[15] S. Palomba, S. Zhang, Y. Park, G. Bartal, X. Yin, and X. Zhang, Nat. Mater. **11**, 34 (2012).
[16] H. Harutyunyan, S. Palomba, J. Renger, R. Quidant, and L. Novotny, Nano Lett. **10**, 5076 (2010).
[17] Y. Shen, *The Principles of Nonlinear Optics* (Wiley-Interscience, New York, 1984).
[18] N. Bloembergen and P. Pershan, Phys. Rev. **128**, 606 (1962).
[19] S. Palomba and L. Novotny, Phys. Rev. Lett. **101**, 056802 (2008).
[20] J. Renger, R. Quidant, N. van Hulst, and L. Novotny, Phys. Rev. Lett. **104**, 046803 (2010).
[21] E. Hendry, P. J. Hale, J. Moger, A. K. Savchenko, and S. A. Mikhailov, Phys. Rev. Lett. **105**, 097401 (2010).
[22] H. Harutyunyan, R. Beams, and L. Novotny, Nat. Phys. **9**, 423 (2013).
[23] S.-Y. Hong, J. I. Dadap, N. Petrone, P.-C. Yeh, J. Hone, and R. M. Osgood, Phys. Rev. X **3**, 021014 (2013).
[24] B. C. Stuart, M. D. Feit, S. Herman, A. M. Rubenchik, B. W. Shore, and M. D. Perry, J. Opt. Soc. Am. B **13**, 459 (1996).
[25] See Supplemental Material at http://link.aps.org/supplemental/10.1103/PhysRevLett.112.056802 for detailed discussion about the TM polarization and laser intensity estimations.
[26] A. D. Rakic, A. B. Djurisic, J. M. Elazar, and M. L. Majewski, Appl. Opt. **37**, 5271 (1998).